

Volume 2, Number 2, pp. 313-320, 2000.



Myocardial Anisotropy Dependent Changes on Torso Currents and Magnetic Fields

C. Ramon*, Y. Wang**, P. Schimpf***, J. Haueisen***, S. Jaruwatanadilok*, and A. Ishimaru*

* Department of Electrical Engineering, University of Washington, Seattle, WA, U.S.A.

*** Rosetta Inpharmatics, Inc., Kirkland, WA 98034, U.S.A.

**** Department of Computer Science, Eastern Washington University, Cheney, WA, U.S.A.

**** Biomagnetics Center, F. S. University, Jena, Germany

Abstract. Changes in torso current flow and magnetic field due to myocardial anisotropy were examined using an anatomically realistic finite element model of an adult male subject. The myocardial fiber orientation in the heart wall was included. The fiber orientations from the canine heart which are available in the literature were mapped to our adult male subject's human heart using deformable mapping techniques. The current and potential distributions in the whole torso were computed using a dipolar source in the septum, left ventricular wall or the right ventricular wall. For each dipole position two cases were studied. In one case the myocardium was isotropic and in the other it was anisotropic. It was found that the current density distribution shows a very noticeable difference between the isotropic and anisotropic myocardium for all dipole positions. The resultant magnetic field in front of the torso was computed using Biot-Savart law. It was found that magnetic field profiles were also affected by the myocardial anisotropy for all dipole positions.

Keywords: Myocardial Anisotropy, Torso Magnetic Fields, Torso Potentials, Torso Models

Introduction

In a recent study we have shown that myocardial anisotropy affects the current flow patterns for a dipolar source in the septum of the heart wall [1]. The results reported here are an extension of our work. Torso current flow patterns and magnetic fields were computed using dipolar sources in different areas of the heart, such as septum, left ventricular wall (LV) and right ventricular wall (RV). It was found that for all three dipolar positions the current flow patterns and the magnetic fields were influenced by the myocardial fiber anisotropy. These results confirm the earlier suggestions made in the literature [2, 3] that myocardial fiber orientations could influence the current flow patterns in the heart and torso. These findings suggest that the orientations of the cardiac muscle fibers should be included in the heart-torso models for an accurate modeling of the volume current distribution in the heart and torso, and also for improved modeling of the torso potentials and magnetic fields. We have used a

highly heterogeneous model of the heart and torso that includes the major tissue types and myocardial fiber orientations [1, 4, 5]. Details of our methods, results, and a discussion are given in the following sections.

Methods

Our procedures for building the heart-torso model and for computing the current distribution and the magnetic field profiles are described elsewhere [1, 4, 5]. A brief review of our methods is given here. We used magnetic resonance imaging (MRI) data of an adult male subject without any known heart problems to construct a high resolution model of the heart and torso. MRI data were collected at the University of Washington Medical Center, Seattle, WA with a GE Signa 1.5 Tesla MRI machine. Each proton density MRI slice was collected with cardiac gating to reduce the motion artifacts. The MRI data were collected when the heart was in the diastolic state. The entire scan consisted of 52 transaxial slices with 6 mm vertical separation. Each slice has a 256x256 pixel resolution. In order to increase vertical resolution of the model, an additional 51 images were generated between the original slices by linear interpolation, resulting in a total of 103 images with 3 mm vertical separation. Similarly, resolution in each slice was increased to 512x512 pixels with a resolution of 0.078x0.078 cm. This was done to provide a better resolution for insertion of the electrical sources in the finite element model of the heart. A semi-automatic tissue classification software was used to segment images. A total of 19 different tissue types were identified in the whole torso.

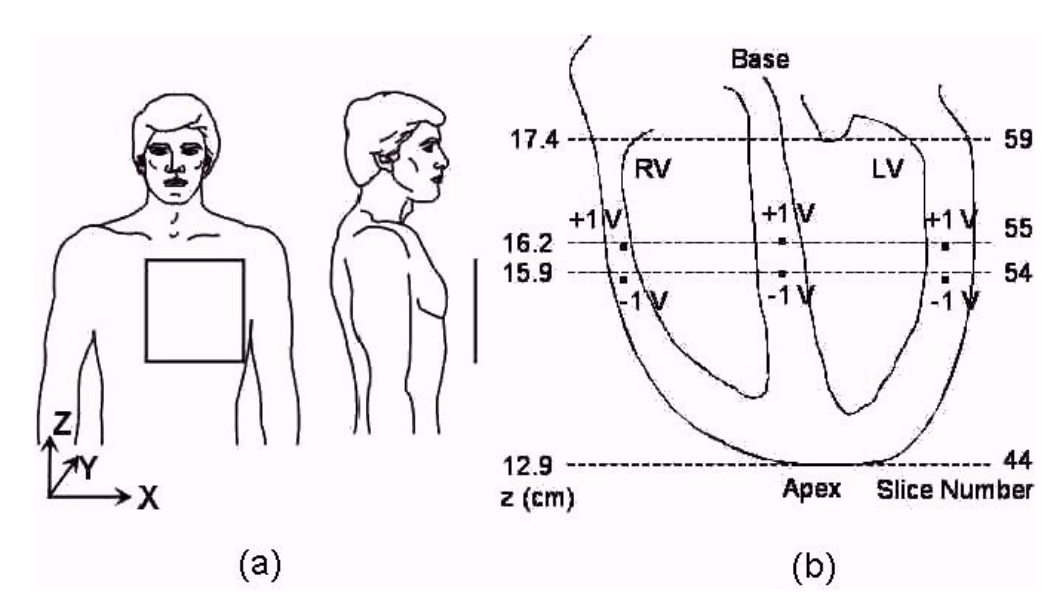


Figure 1. (a) A layout of the torso shape, the orientation of the coordinate system and the location of the planar sampling surface for the magnetic fields; (b) details of the image slices in the heart area and the location of the dipolar sources in the septum, LV and RV wall

A layout of the torso surface, coordinate orientation, and the sampling surface in which the magnetic field profiles were computed is shown in figure 1(a). A schematics of the heart wall, the image slices in the heart and the location of dipoles are shown in figure 1(b). The increasing x direction is from the right side of the subject to the left, the increasing y direction is from front (anterior) to the back (posterior) of the subject, and the increasing z direction is from the abdomen (inferior) to the shoulders (superior). The first image slice of the torso, i.e., slice number 1, is located at the z=0 cm at the upper abdomen area. The last image slice, i.e., slice number 103, is located at z=102x0.3= 30.6 cm at the upper chest area. As shown in figure 1(b), the bottom of the heart, i.e., apex, is located in slice number 44 at z=12.9 cm. The top of the ventricles is in slice number 59, and the top of the heart is located in slice number 67 at z=19.8 cm, which is not shown in the figure.

A complete data set of ventricular fiber orientation for the human heart is unavailable in the literature. However, it has been found that heart fiber structure is very similar across various mammalian species [2]. A complete data set of the fiber orientation in a canine heart has been mapped at the University of Auckland in New Zealand [6], and it is available at their web site on the Internet. This data set is being used by other research groups for incorporating the fiber anisotropy into computer models of the heart [7, 8]. We mapped the fiber orientations from the canine heart to our adult male subject's human heart using deformable mapping techniques [7].

A finite element mesh with rectangular parallelopiped (brick-shaped) elements was generated in the whole torso. We used the smallest elements of the size 0.078x0.078x0.3 cm in the heart wall and larger size elements in other parts of the torso. An adaptive finite element solver developed by us was used for all the computational work [9]. A dipole of +1 and -1volt was placed between slices 55 and 54 in the septum. Similar dipole locations were used in the RV and LV wall. Only one dipole was used in each simulation. These are idealized dipoles for computer simulations only and do not represent any cardiac activation. The choice of +1 and -1 volt was used so that computed results can be easily scaled to other values. The potential and current distributions in the whole torso were computed for two cases using the dipole as a boundary condition. In one case the anisotropic myocardial tissue resistivities, and in the other case the isotropic myocardial tissue resistivities, were used. Isotropic tissue resistivities were used for all other tissue types and were kept the same in both cases. These resistivity values are available in the literature and have been used earlier by us [1, 4, 5]. Using Biot-Savart law, the magnetic field outside the torso is computed from the primary currents flowing in the dipolar source and secondary volume currents in the whole torso. The magnetic field profiles were computed in a planar sampling surface located at 1.0 cm in front (anterior) of the torso of the subject. The size of the sampling surface is 20x20 cm and the sampling points were on a 40x40 grid. This gives a grid spacing of 0.5x0.5 cm. A layout of the sampling surface is shown in figure 1(a). The sampling surface extends from 5 to 25 cm in the z direction and from 11 to 31 cm in the x direction.

All computations were performed on an Intel Pentium II, 350 MHz, 2 CPU, 512 MB memory workstation running a Linux operating system. An average run took about 30 minutes for computing the potential and current distribution in the whole torso. The post-processing and visualization of the data were done using Matlab 5.3 software (Mathworks, Inc., Natick, MA).

Results

Torso Current Flow PatternsThe current density (A/cm²) distribution in a slice is shown in figure 2 for a dipole in the septum. Slice number 59 was chosen for showing the current distribution. It is four slices above the dipolar source. This particular slice was chosen for display of the current density distribution because it is away from the tip of the dipole, and current flow from the dipole has enough space to spread out. However, any other slice would have been equally good as a representative slice for the display of the current density distribution. The plots are shown for the anisotropic and isotropic cases, and for the difference between the two. The upper row of the plots is for the whole slice, and the bottom row of the plots is for a magnified view in the heart and surrounding areas. The maximum and minimum values of the contours and the separation, dj, between the contour lines are given in the plots.

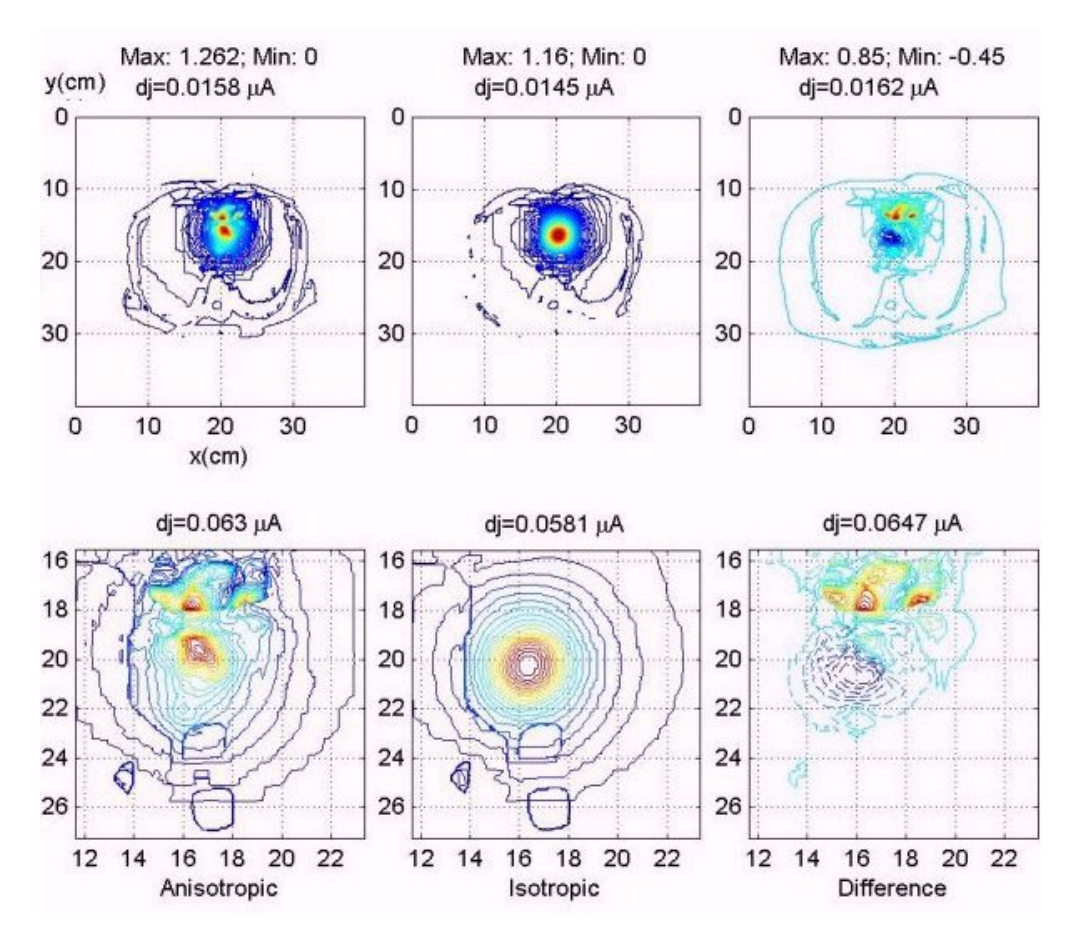


Figure 2. Contour plot of the current density distribution in one of the image slices for a dipole in the septum. Top row of the plots is for the whole torso slice and the bottom row of the plots is for the details in the heart area. Plots are for the anisotropic, isotropic, and the difference between the two cases. The current density distribution for the anisotropic myocardium shown in the left bottom plot has more structural pattern as compared to the isotropic case shown in the middle bottom plot. Both plots are remarkably different. The contour lines seem to be almost circular for the isotropic case with one noticeable peak in the center. For the anisotropic case there seems to be many peaks and valleys. These are more recognizable in the difference plot at the bottom right. The difference between the anisotropic and isotropic case shown in the right top and bottom plots seems to have a pattern of current distribution similar to the anisotropic case. This would suggest that in the vicinity of the heart the current flow pattern is significantly influenced by the myocardial anisotropy. In the difference plot, the positive contour lines are shown with solid lines and the negative ones with dashed lines. The current density distribution has distinct contour lines at some of the tissue boundaries. This is expected because at some of the tissue boundaries the resistivity values are significantly different from one another, which will change the current flow in a very noticeable fashion. Examples of these are the spinal column and the surrounding tissues, and at the boundaries of lungs, fat, bones and muscles. It is more noticeable in the difference plots. This implies that the difference plots are more dominated by the anisotropic current density distribution as compared to the isotropic one. The details of the difference of the current density distribution in the heart area are given in the magnified views in the bottom right plot. Due to the myocardial anisotropy in the heart wall, the differences in the current distribution are more pronounced and complex as compared to the other areas of the torso. To quantify the differences, the correlation coefficient between the anisotropic and isotropic current density distribution was computed. For the current density distribution shown in Figure 2 it is 0.92.

The correlation coefficients for other slices were also computed, and these are plotted in figure 3. Slices containing the heart are from 44 to 67. The correlation coefficients for the

slices in the heart area have lower values for the dipoles in the septum and LV wall, suggesting that the myocardial anisotropy influences the current flow very strongly within the heart and in the vicinity of the heart area for these dipoles. Moving away from the heart, either towards the upper chest area or the lower lungs and abdomen area, the correlation coefficient is in the range of 0.97 to 0.99. This would suggest that the current density distribution is affected slightly by the myocardial anisotropy in the torso areas away from the heart. One reason could be that isotropic conductivities of the other tissues in the upper and lower torso smooth out the anisotropy dependent current flow patterns coming out of the heart wall. The correlation coefficient for the dipole in the RV wall shows a different pattern as compared to the dipoles in the septum and LV wall. It is higher for the slices containing heart and lower for the slices in other parts of the torso.

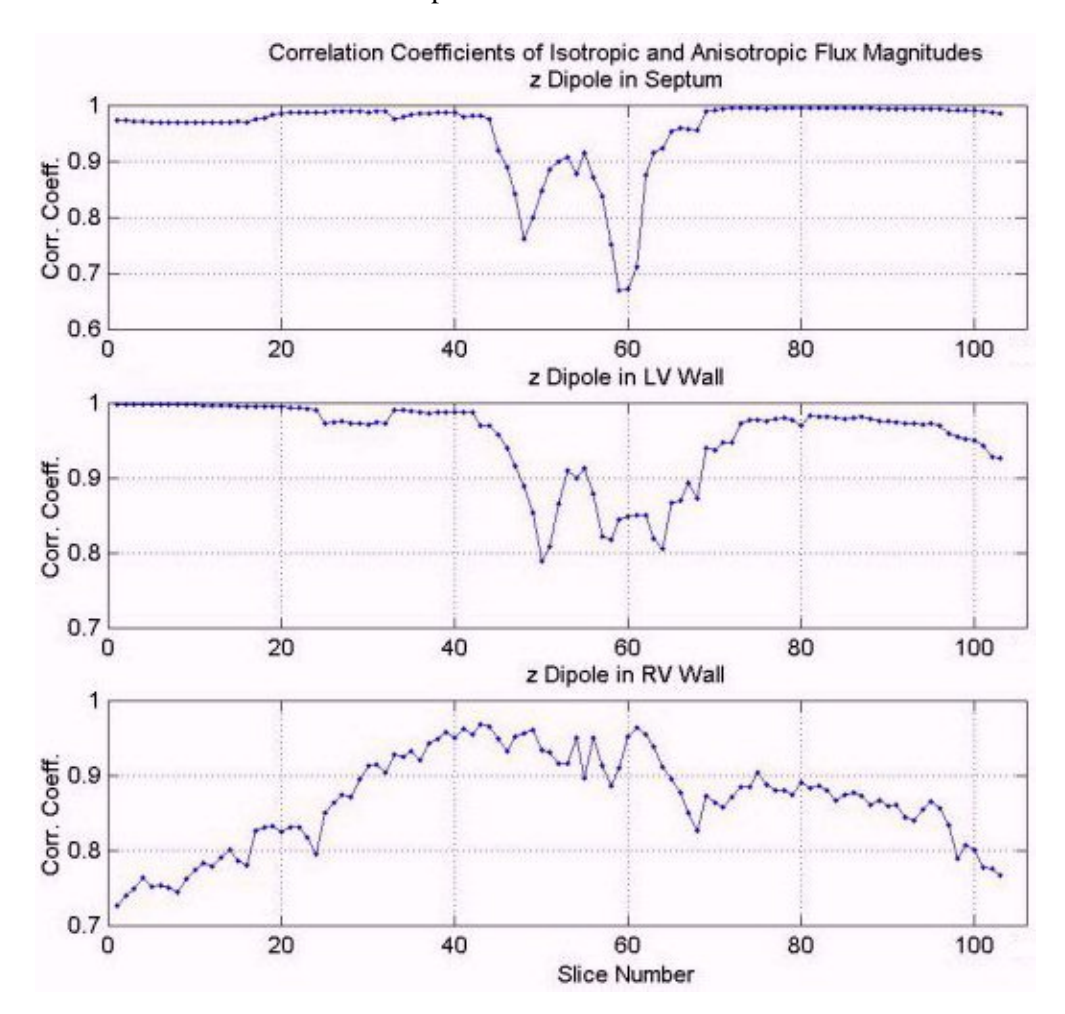


Figure 3. Correlation coefficients of the anisotropic and isotropic current density distribution for all the slices of the torso model.

Torso Magnetic Field Profiles

Figure 4 shows the contour plot of the y component (~ normal to the torso) of the magnetic field in a planar sampling surface for the dipole in the septum. It shows the field plots for the isotropic, anisotropic and the difference of the two plots. The maximum and minimum peak values, and the separation between the contours, dB, for all the plots are given. The contour plots show a pattern similar to the magnetic field of a dipolar source which are characterized by the symmetrically placed positive and negative contour peaks with respect to the zero crossing line. This fits well because the source is a dipole oriented in the z direction, and thus the y component of the magnetic field will be similar to the contour plot of a dipolar source.

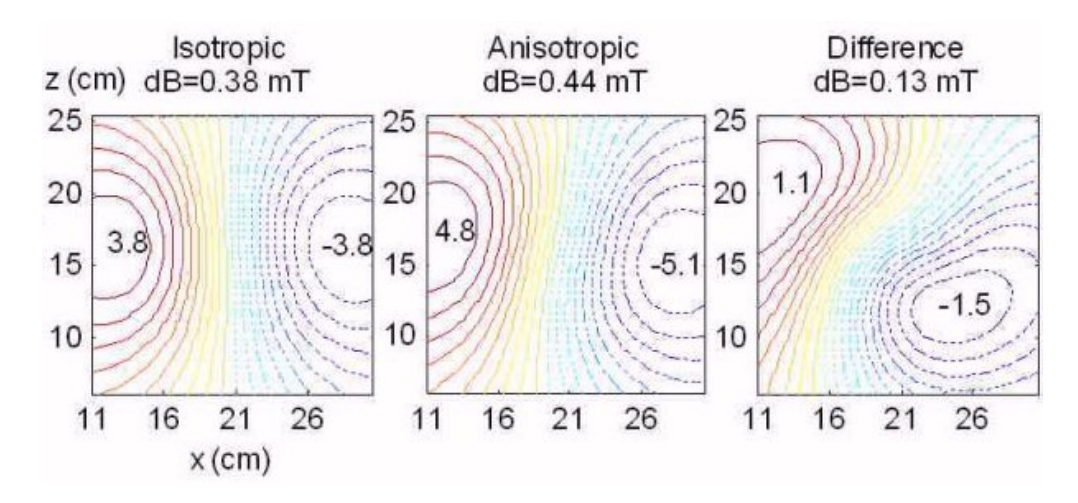


Figure 4. Contour plots of the normal component of the magnetic field for a dipole in the septum. Plots are for isotropic, anisotropic, and the difference of the two.

For the dipole in the septum (figure 4), the correlation coefficient of the anisotropic and isotropic magnetic field profiles is 0.98. This would suggest that the anisotropic and isotropic magnetic fields are only slightly different from each other with some noticeable differences in the contour patterns. The zero-crossing contour lines are almost vertical for the isotropic case, while for the anisotropic case they are slightly tilted towards the right. These features are more pronounced in the difference contour plot. The maximum and minimum peak values are also different for the two cases. Please note that spatial location of the peaks are at slightly different positions for isotropic, anisotropic and the difference magnetic field plots. In general, the differences between the isotropic and anisotropic cases are recognizable.

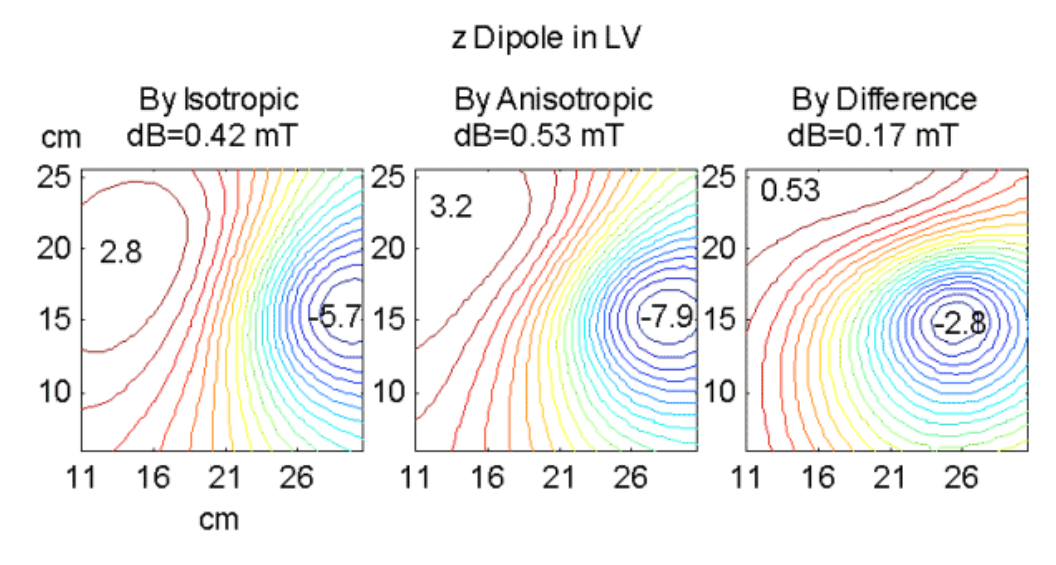


Figure 5. Contour plots of the normal component of the magnetic field for a dipole in the LV wall. Plots are for isotropic, anisotropic, and the difference of the two.

Figure 5 shows the contour plots of the anterior magnetic field for the dipole in the LV wall. Profiles of the plots and the location of the peaks are different as compared to the dipole in the septum. The correlation coefficient for the anisotropic and isotropic magnetic field profiles is 0.98 for the LV dipole. It is the same as for the dipole in the septum.

z Dipole in RV

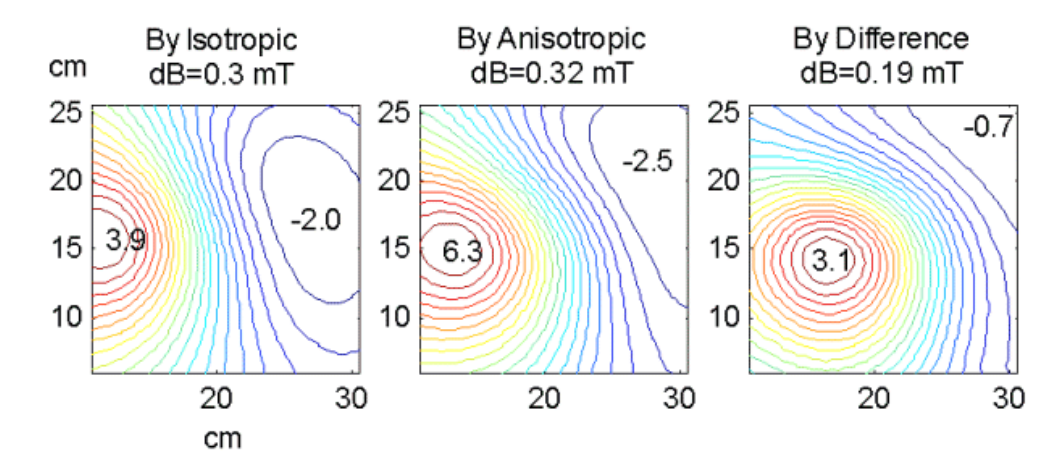


Figure 6. Contour plots of the normal component of the magnetic field for a dipole in the RV wall. Plots are for isotropic, anisotropic, and the difference of the two.

Figure 6 shows the contour plots of the anterior magnetic field for the dipole in the RV wall. It is significantly different as compared to the plots shown in figures 4 and 5. This suggests that the myocardial anisotropy significantly affects the torso magnetic fields for the dipolar source in the RV wall. The correlation coefficient for the anisotropic and isotropic magnetic field profiles is 0.96 for the RV dipole.

Conclusions

These results show that the myocardial anisotropy influences the current flow patterns and torso magnetic fields very strongly. Effects on the current flow patterns are more significant in the heart and in the surrounding tissue areas for the dipole in the septum and the LV wall. For the dipole in the RV wall, the pattern of the correlation coefficients is opposite as compared to the dipoles in the septum and LV wall. It has higher values for the slices in the heart area as compared to the other parts of the torso. This could be one reason that the magnetic field of the RV dipole is more affected by the myocardial anisotropy as compared to the magnetic field of the dipoles in the septum and LV wall. The torso magnetic fields show some noticeable differences, but not very large differences. Even a slight difference in the magnetic field profile would influence the localization of the sources while solving the biomagnetic inverse problem. It has been observed before that a correlation coefficient of 0.98 will yield an average of 0.5 to 0.8 cm localization errors and a maximum of up to 1.5 cm localization errors [10]. These results would suggest that the myocardial anisotropy should be included in the anatomically realistic models of the heart and torso for computer modeling of the electrical activity of the heart.

Acknowledgements

This research was partially supported by a National Science Foundation grant number INT-9726712 and an NIH grant number RR13301-01, and an equipment grant from the Seattle Foundation.

References

- [1] Ramon, C., Wang, Y., Haueisen, J., Schimpf, P., Ishimaru, A. and Jaruvatanadilok, S., "Effect of myocardial anisotropy on torso current flow patterns and magnetic fields", Phys. Med. Biol., 45, 1141-1150, 2000.
- [2] Streeter Jr., D. D., "Gross morphology and fiber geometry of the heart", in Handbook of Physiology: A critical, comprehensive presentation of physiological knowledge and concepts, vol. I, Ed: R. M. Berne (American Physiological Society, Bethesda, MD, U.S.A.), pp. 61-112, 1979.
- [3] Taccardi, B., Lux, R. L., Ershler, P. R., Macleod, R., Dustman, T. J. and Ingebrigtsen, N., "Anatomical architecture and

- electrical activity of the heart", Acta Cardiol., 52, 91-105, 1997.
- [4] Ramon, C., Czapski, P., Haueisen, J., Huntsman, L. L., Nowak, H., Bardy, G. H., Leder, U., Kim, Y. and Nelson, J. A., "MCG simulations with a realistic heart-torso model", IEEE Trans. Biomed. Engr., 45, 1322-1341, 1998.
- [5] Schimpf, P., Haueisen, J., Ramon, C. and Nowak, H., "Realistic Computer Models of Electric and Magnetic Fields of Human Head and Torso", Parallel Computing, 24, 1433-1460, 1998.
- [6] Nielsen, P. M. F., Le Grice, I. J., Smaill, B. H. and Hunter, P. J., "Mathematical model of geometry and fibrous structure of the heart", American Journal of Physiology, 260, H1365-1378, 1991.
- [7] Wang, Y., "Analysis of defibrillation efficacy and investigation of impedance cardiography with finite element models incorporating anisotropic myocardium", Ph.D. dissertation, University of Washington, Seattle, WA, U.S.A, 1999.
- [8] Eason, J., Schmidt, J., Dabasinskas, A., Siekas, G., Aguel, F. and Trayanova, N., "Influence of anisotropy on local and global measures of potential gradient in computer models of defibrillation", Ann. Biomed. Engr. 26. 840-849, 1998.
- [9] Schimpf, P. H., Haynor, D. R. and Kim, Y. "Object-free adaptive meshing in highly heterogeneous 3-D domains", Int. Jour. of Biomedical Computing, 40, 209-225, 1996.
- [10] Haueisen, J., Bottner, A., Nowak, H., Brauer, H. and Weiller, C., "The influence of conductivity changes in boundary element compartments on the forward and inverse problem in Electroencephalography and Magnetoencephalography", Biomedical Engineering, 44, 150 - 157, 1999.



Official journal of the International Society for Bioelectromagnetism